Journal of Volcanology and Geothermal Research 415 (2021) 107250

Contents lists available at ScienceDirect

Journal of Volcanology and Geothermal Research

journal homepage: www.elsevier.com/locate/jvolgeores

Insight into the May 2015 summit inflation event at Kīlauea Volcano, Hawai'i

Mark J.W. Bemelmans [a,*,1], Elske de Zeeuw- van Dalfsen [a,b], Michael P. Poland [c], Ingrid A. Johanson [d]

[a] Delft University of Technology, Delft, the Netherlands
[b] Royal Netherlands Meteorological Institute (KNMI), De Bilt, the Netherlands
[c] U.S. Geological Survey Cascades Volcano Observatory, Vancouver, Washington, USA
[d] U.S. Geological Survey Hawaii Volcano Observatory, Hilo, Hawaii, USA

ARTICLE INFO

Article history:
Received 19 October 2020
Received in revised form 8 April 2021
Accepted 10 April 2021
Available online 17 April 2021

Keywords:
Kīlauea summit intrusion
Volcano geodesy
InSAR time series

ABSTRACT

We use ground and space geodetic data to study surface deformation at Kīlauea Volcano from January to September 2015. This period includes an episode of heightened activity in April and May 2015 that culminated in a magmatic intrusion beneath the volcano's summit. The data set consists of Global Navigation Satellite System (GNSS), tilt, visual and seismic time series along with 25 descending and 15 ascending acquisitions of the Sentinel-1 satellite. We identify four different stages of surface deformation and volcanic activity, which we attribute to pressure changes and the movement of magma in response to an imbalance between magma supply and withdrawal in the shallow plumbing system, eventually leading to an intrusion beneath the summit area. In particular, we model the deformation as due to pressure changes in two subsurface magma bodies: the Halema'uma'u Reservoir (HMMR) and South Caldera Reservoir (SCR). The SCR was best described by an ellipsoidal source at 2.8 (2.65–3.07 at 95% confidence) km depth below the south caldera region. The HMMR was modeled as a point source located just east of Halema'uma'u crater at 1.5 (0.95–2.62) km depth. We suggest that a short-term increase in the magma supply rate to the volcano is a potential mechanisms for the intrusion, although other factors, like the filling of available void space or a reduced efficiency of magma transport through the volcano's East Rift Zone, may also play a role.

1. Introduction

Kīlauea Volcano, located on the Island of Hawai'i, is one of the most active volcanoes on Earth. The volcano erupted continuously from the Pu'u 'Ō'ō vent along the volcano's East Rift Zone (ERZ) from 1983 to 2018 (Patrick et al., 2019), and from 2008 to 2018 a lava lake was present inside Halema'uma'u crater in the summit region (Poland et al., 2014; Neal et al., 2019). Kīlauea's extensive monitoring network (Fig. 1) consists of dozens of continuously measuring Global Navigation Satellite System (GNSS) receivers, tilt instruments, and seismometers. Additionally, a thermal camera was pointed at the summit lava lake to record the lava level with respect to the vent rim. This network supports not only monitoring but also facilitates more detailed study of the volcano's magmatic system.

Geodetic data have long shown multiple sources of persistent volume and mass changes beneath the volcano's summit (e.g. Fiske and Kinoshita, 1969; Johnson et al., 2010; Baker and Amelung, 2012; Bagnardi et al., 2014), suggesting a complex magma plumbing system that consists of at least two main magma storage areas: a shallow "Halema'uma'u" reservoir about 1–2 km beneath the caldera center, and a deeper "south caldera" storage area about 3–5 km beneath the south part of Kīlauea caldera (Poland et al., 2014). We refer to these storage areas as Halema'uma'u reservoir (HMMR) and south caldera reservoir (SCR). Here we focus on changes in magma storage associated with a summit intrusion in May 2015.

Magma supply to Kīlauea varies with time. From 2003 to 2007, for example, the magma supply rate temporarily increased by almost 50% (Poland et al., 2014; Anderson and Poland, 2016). This period was followed by a relative lull, reaching a low point around 2010–2012 (Anderson and Poland, 2016; Dzurisin and Poland, 2018). From 2012 to 2015 magma supply likely returned gradually to pre-2003 levels (Dzurisin and Poland, 2018). Throughout all these periods a connection between the summit and ERZ was maintained, feeding the 1983–2018 eruption on the volcano's flank (Patrick et al., 2019). In this context it is important to note that during the May 2015 event, no significant changes were noted in the style of the ERZ eruption (Patrick et al., 2019).

The May 2015 intrusion is of special interest because: 1) the activity involved both the south caldera and Halema'uma'u magma storage areas beneath the summit region, 2) it was associated with an overflow of the summit lava lake, and 3) it was observed by modern monitoring techniques. Although common prior to 1983, intrusions beneath the

* Corresponding author.
E-mail address: mark.bemelmans@bristol.ac.uk (M.J.W. Bemelmans).
[1] Now at University of Bristol, Bristol, United Kingdom.

https://doi.org/10.1016/j.jvolgeores.2021.107250
0377-0273/

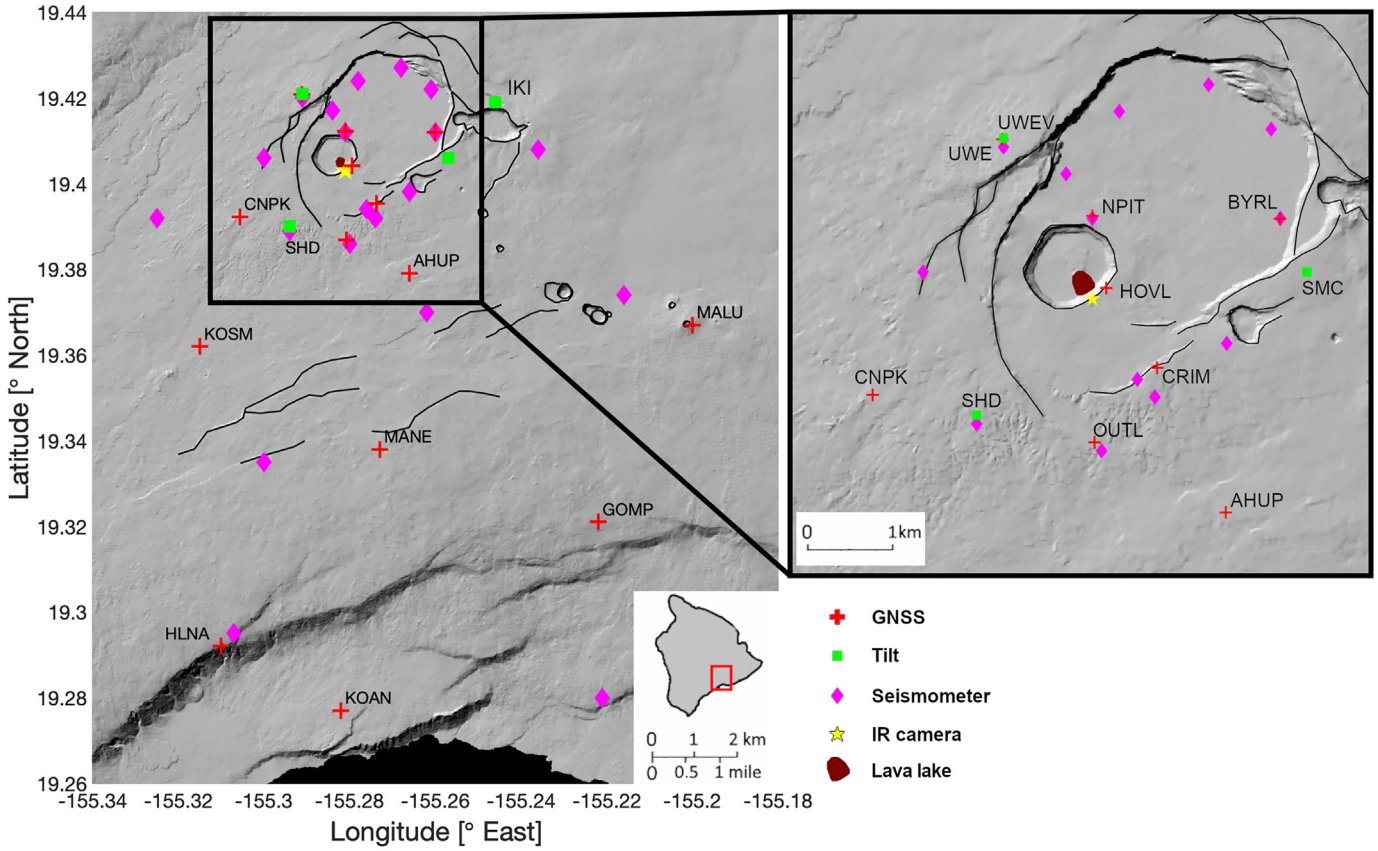

Fig. 1. Locations of monitoring instruments used for this research. Red "+"-signs are GNSS stations with their 4-letter names indicated, green squares are tiltmeters depicted with their 3-letter names, and magenta diamonds are seismometers. The infrared camera is located at the yellow star and was pointed at the lava lake, which is shown in dark red. Inset shows location of the region on the Island of Hawai'i. Thin black lines show important geomorphological features, like the caldera boundary. When possible the same features are shown in other figures in this paper. For clarity some instruments are only labeled in the zoom of the caldera region.

summit area were rare after that time, and none had occurred since the advent of GNSS or Interferometric Synthetic Aperture Radar (InSAR), both of which can provide detailed observations of ground displacement. The 2015 episode, therefore, provides a unique opportunity to apply modern geodetic data sets and modeling techniques to improve our understanding of summit magmatism at Kīlauea, including interactions between the different parts of the magma plumbing system and the mechanisms for intrusive activity–information of vital importance as the volcano recovers from its 2018 collapse (Neal et al., 2019; Poland et al., 2019).

Jo et al. (2015) modeled COSMO-SkyMed InSAR data spanning the May 2015 summit intrusion and concluded that a volume change associated with the SCR explains their observations, but little other attention has been paid to this noteworthy event and its implications. We utilize both ground- and space-based geodetic data, along with observations of earthquake and lava lake activity, to better understand the sequence of events in April and May 2015 that led to the summit intrusion, the timing of magma transfer between summit storage areas, and the possible mechanisms for the intrusion. Our particular focus is on the Sentinel-1 InSAR data set, which provides important information on the geometry, timing, and magnitude of magma transport.

1.1. Event chronology

The May 2015 event can be divided into four stages (A-D) based on seismic, tilt and lava lake data (Fig. 2).

During stage A, April 21 to April 29, a 40 m rise in lava level occurred along with inflationary tilt. These signals are commonly associated with pressurization of the HMMR located beneath the eastern edge of Halema'uma'u crater (Poland et al., 2014; Anderson et al., 2015). An increase in seismic activity in the summit area is also consistent with magma pressurization (Traversa and Grasso, 2010). In stage B, April 30 to May 9, seismic activity remained elevated and only minor changes in tilt were detected. At the same time, the lava level overtopped the vent rim, repeatedly flowing onto the floor of Halema'uma'u crater. Stage C, May 10 to May 12, saw a 30 m drop in lava level coincident with deflationary tilt, indicating depressurization of the HMMR. The final stage D, May 13 to May 17, was characterized by a spike in seismic activity in the summit area, mainly focused in the south caldera and the upper part of the Southwest Rift Zone (SWRZ). There was no significant change in the radial tilt, but a sharp jump in the tangential tilt of the UWE station occurred, indicating that it was not the Halema'uma'u source but another source that was active. This stage also saw a further 30 m drop in lava level. From May 18, seismic activity, variations of tilt, and lava level returned to normal levels and patterns as observed before the May 2015 event.

Changes in summit magma storage have often been associated with changes in eruptive activity from the ERZ. During April–May 2015, however, no changes were noted in the ERZ lava effusion rate. It seems that magma transport to the ERZ was not impacted by, nor did it impact, the summit during the anomalous April–May 2015 event.

2. Data analysis

In the following section, we present and analyse earthquake hypocenters, GNSS displacements, tilt measurements, lava lake observations, and InSAR acquisitions covering the May 2015 intrusion.

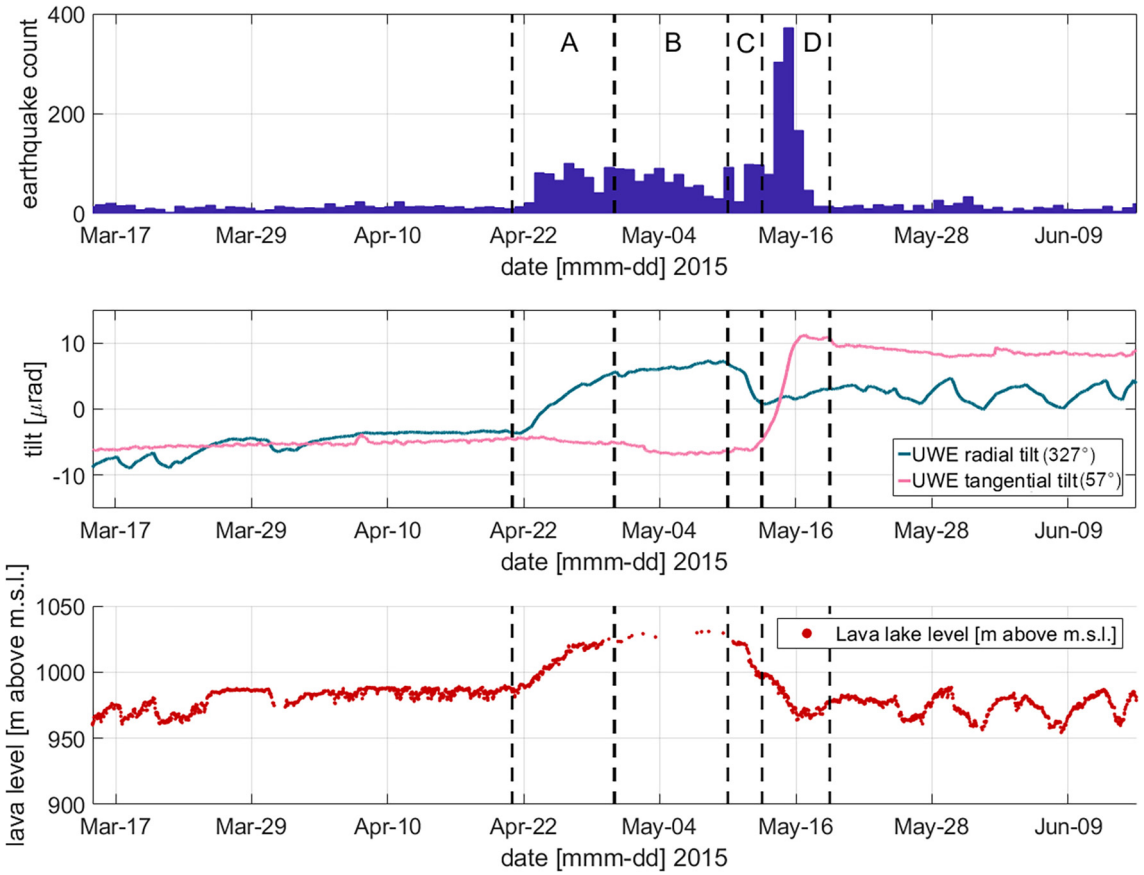

Fig. 2. Time series of seismic, tilt, and lava level data from March 15, 2015, to June 15, 2015. Top: Number of earthquakes per day in the general area of the summit caldera and upper ERZ. Middle: Radial and tangential tilt from station UWE. Orientation given in degrees clockwise from North. Bottom: Variation in lava lake level determined from infrared camera images. The vertical dashed lines indicate different stages of the May 2015 intrusion.

2.1. Earthquake hypocenters

From March 15 to June 15, 2015, 3099 earthquakes with depths of less than 10 km were recorded beneath the caldera and upper ERZ. These shallow earthquakes are mostly linked to pressure changes within the magma plumbing system of the volcano [Klein et al., 1987; Wauthier et al., 2016]. Nearly half of these earthquakes occurred during April 21–May 17.

Background seismic activity (Fig. 2), characterized by numerous seismometers in the summit region (Fig. 1), was <10 earthquakes per day. Seismic activity stayed above background for the entirety of the May 2015 event (our stages A-D), with the peak of >200 earthquakes per day coinciding with the south caldera inflation stage (D) of the May 2015 event.

The histograms for each of the regions in Fig. 3 allow us to track the location of earthquake activity over time. Seismicity shifted from the main caldera to the UERZ and back before shifting to the south caldera region and increasing in intensity. In the main caldera region (box 1 in Fig. 3), the seismic activity occurred primarily during stages A and C, which correlates with inflation and deflation of the summit caldera respectively. The depth histograms show that, in all regions events are shallow, with a mean of about 2 km. This matches with the inferred depths of the summit reservoirs (Poland et al., 2014). However, we note that the depth of seismicity is not necessarily reflective of magma storage depths (Wauthier et al., 2016, 2019).

2.2. GNSS displacements

The GNSS displacement patterns recorded by the 9 stations located in the summit region (Fig. 1) show how surface deformation varied through time (Fig. 4). Stage A is characterized by inflation centered slightly east of Halema'uma'u crater – the proposed location of the HMMR (Cervelli and Miklius, 2003; Baker and Amelung, 2012; Bagnardi et al., 2014; Poland et al., 2014; Anderson et al., 2015; Patrick et al., 2015; Wauthier et al., 2019). Deformation during stage B is not as strong as during the other stages and is centered close to Keanakāko'i Crater in the southeast part of the caldera. Stage C sees deflation centered in the same location as the inflation during stage A. Finally, stage D has significantly larger displacements centered on the southern edge of the caldera, which coincides with the proposed location of the SCR. The OUTL station is closest to the area of maximum vertical displacement, with about 11.5 cm of uplift and almost no lateral displacement.

Surface deformation can be linked to changes in pressure of multiple magma reservoirs. For stages A and C this is the HMMR, and for stage D the SCR. For stage B, this could be the Keanakāko'i reservoir, a temporary magma storage reservoir proposed by Poland et al. (2014); however, given the small amount of deformation that occurred during this stage, magma storage in this area remains ambiguous.

2.3. Tilt

Tilt is measured at four locations in Kīlauea's summit region (Fig. 1). Two stations in particular, UWE and SDH, show a clear response to all stages of the May 2015 event (Fig. 5).

Tiltmeters at the summit are characterized by an increase in radial tilt when the HMMR inflates. These tilt changes are best recorded by the UWE station, which also often captures transient deflation-inflation - or DI - events (Anderson et al., 2015), visible as sawtooth patterns in Fig. 5. The progression of the radial tilt from the UWE tiltmeter

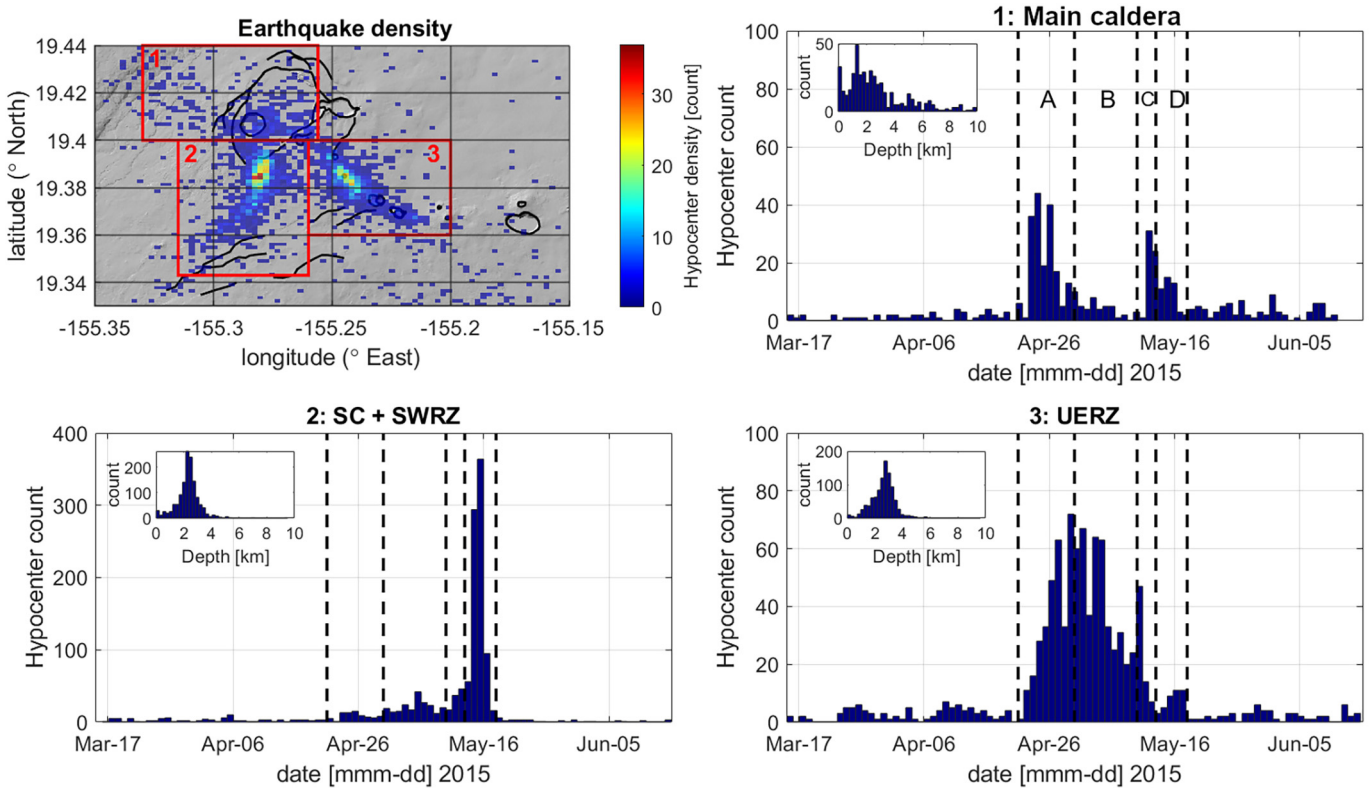

Fig. 3. Earthquake density map showing the number of earthquakes per day between March 15 and June 152,015. The red boxes marked 1, 2, and 3 show the geographical extent of the regions represented in each of the histograms (1, 2 and 3). SC = South caldera, SWRZ = Southwest Rift Zone, UERZ = Upper East Rift Zone, also referred to as the east rift connector (Swanson et al., 2018). Note that the vertical scale of the SC + SWRZ histogram extends to higher values than that of the main caldera and UERZ. The inset panels on each of the histograms show the depth distribution of the earthquakes in that region.

shows inflationary tilt during stage A and deflationary tilt during stage C, with little change during stages B and D. The only significant change in tangential tilt was a large jump (15 microradians) during stage D. At SDH, the radial and tangential tilts track those at UWE, but the magnitude of the tangential signal in stage D is much larger – 75 microradians. These tilt patterns provide additional evidence for the inflation and subsequent deflation of the HMMR during stages A and C, and strong inflation of the south caldera during stage D. Almost no change in tilt was recorded during stage B, but the tiltmeter network may not be sensitive to changes in the Keanakāko'i region.

2.4. Lava level

The lava level within the summit eruptive vent fluctuated significantly during April–May 2015. Patrick et al. (2015) showed that variation in lava level at the summit can be used as a simple piezometer for the shallow plumbing system. Applying this to the lava level variation during April–May 2015 provides valuable information on the pressure changes within the shallow plumbing system, in particular the HMMR, which directly fed the lava lake. Fig. 6 shows the variation in lava level during the April–May 2015 activity.

As expected from the surface deformation, a rise in lava level occurred during stage A and a drop in stage C. The lava level remained at the edge of the summit eruptive vent for the duration of stage B. Because of this, the infrared camera could not measure the level of the lava with respect to the crater rim. The continued drop in lava level during stage D indicates that during this period, the pressure in the HHMR dropped further. In total, the lava level dropped about 70 m between the high point during stage B and the lowest level during stage D. Using the geometry of the vent presented in (Carbone et al., 2013) the surface area of the lake is 25,200 m^2. The 70 m drop represents a volume change of about 1.76 million m^3. Careful inspection shows a 24 h stable period on May 13. This coincides with the shift in deformation from the HHMR (stage C) to the south caldera (stage D).

2.5. InSAR

A total of 40 Sentinel-1 Single-Look Complex (SLC) images, 15 ascending and 25 descending, acquired between January and October 2015 were used for InSAR analysis. The topographic correction was performed using the SRTM 30 m Digital Elevation Model (Farr et al., 2007). The interferograms were processed with the Stanford Method for Persistent Scatterers (StaMPS) software (Hooper et al., 2004, 2007). Default settings were used to obtain deformation time series of persistent scatterer pixels (PS pixels) for both ascending and descending data sets. Detailed information on the Sentinel-1 data and data processing is given in the supplementary information (Text S1, S2 and Tables S1, S2).

Sequential descending-orbit interferograms (Fig. 7) show deformation at the summit before and during the May 2015 intrusion event. Due to the temporal resolution of available data, one interferogram covers stage A and a little of B (Fig. 7 left), the other (Fig. 7 right) captures the rest of stage B, stage C and most of stage D. Fig. 7(left) shows uplift corresponding to inflation of the HMMR. Fig. 7(right) shows both subsidence centered inside the caldera, which is linked to deflation of the HMMR, and strong uplift related to inflation of the SCR. Deformation of the south caldera is not radially symmetric, but has a lobe extending toward the east. This lobe is approximately in the direction of the ERZ and could be the result of inflation of the Keanakāko'i reservoir due to temporary magma storage there.

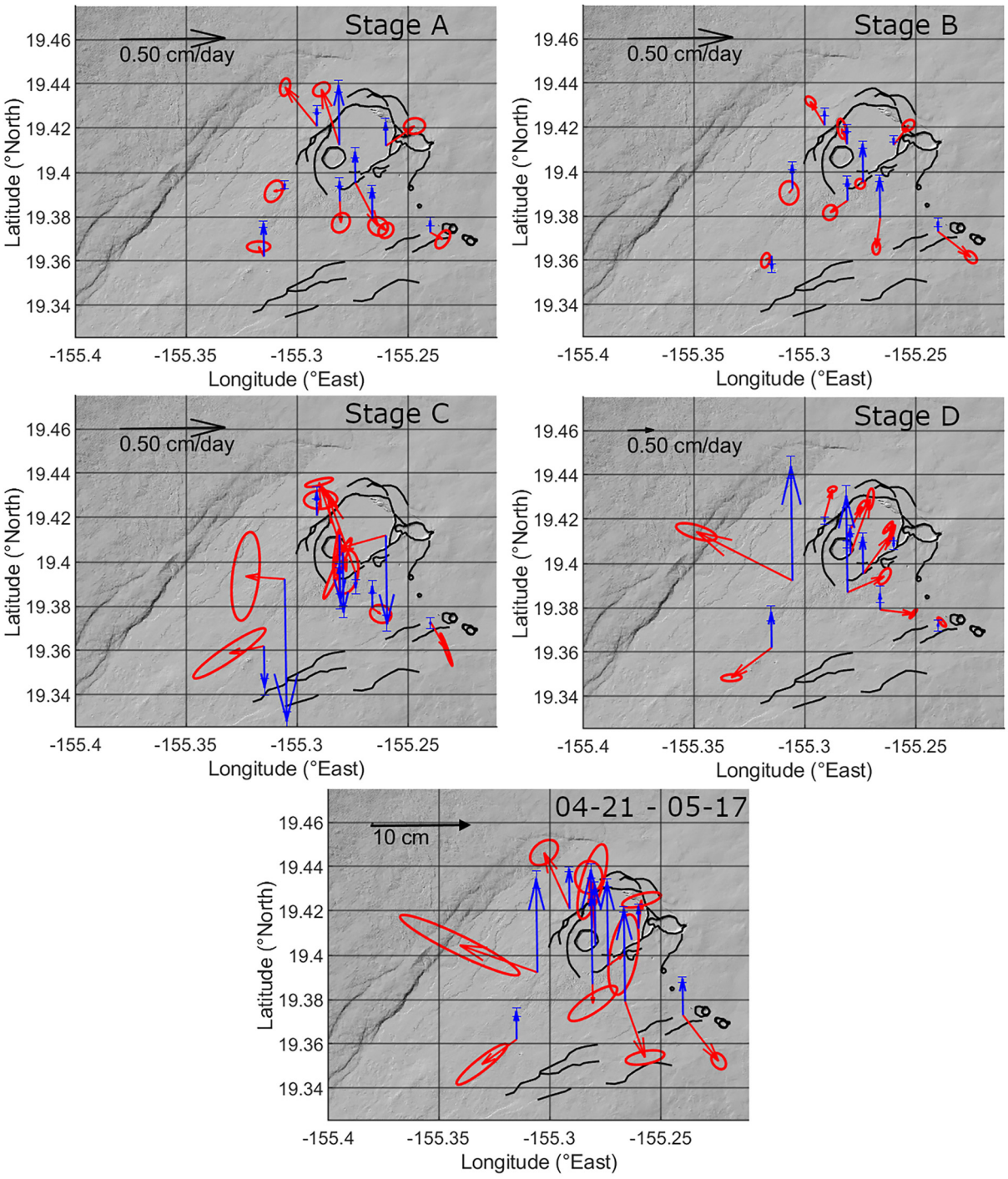

Fig. 4. GNSS displacement rates for each stage of the May 2015 event. Red and blue arrows show horizontal and vertical displacements, respectively. Note that, for stage D, The length of the arrow showing 0.5 cm/day displacement is 4 times smaller compared to the other stages. The bottom panel shows GNSS deformation for the entire event in cm.

From tilt and GNSS data we know that the greatest change in LOS displacement occurred in April/May 2015. This is also visible in both ascending and descending time series of LOS displacement of randomly selected PS pixels (Fig. 8). From the descending stack, it is clear that most deformation occurs between the acquisitions on April 9, 2015 and May 15, 2015. These dates roughly match stages A-D determined from the ground monitoring network. The periods outside this date range do not show significant deformation. The same is true for the ascending stack, with most deformation occurring between May 6, 2015 and May 18, 2015. The overall deformation associated with the April–May 2015 event can be estimated by determining the least squares difference in LOS displacement that occurred between the stable periods before and after the activity. Owing to the lack of pre-event acquisitions on the ascending track, we estimated displacements over February 11, 2015 to June 11, 2015. On the descending track, we estimate the displacements that occurred over April 9, 2015 to June 8, 2015. Although the calculations do not span the exact same time periods, the displacements before and after the April–May 2015 activity are comparatively minor, and thus should not significantly influence the LOS displacement associated with the event. For each PS pixel, we estimate the overall LOS

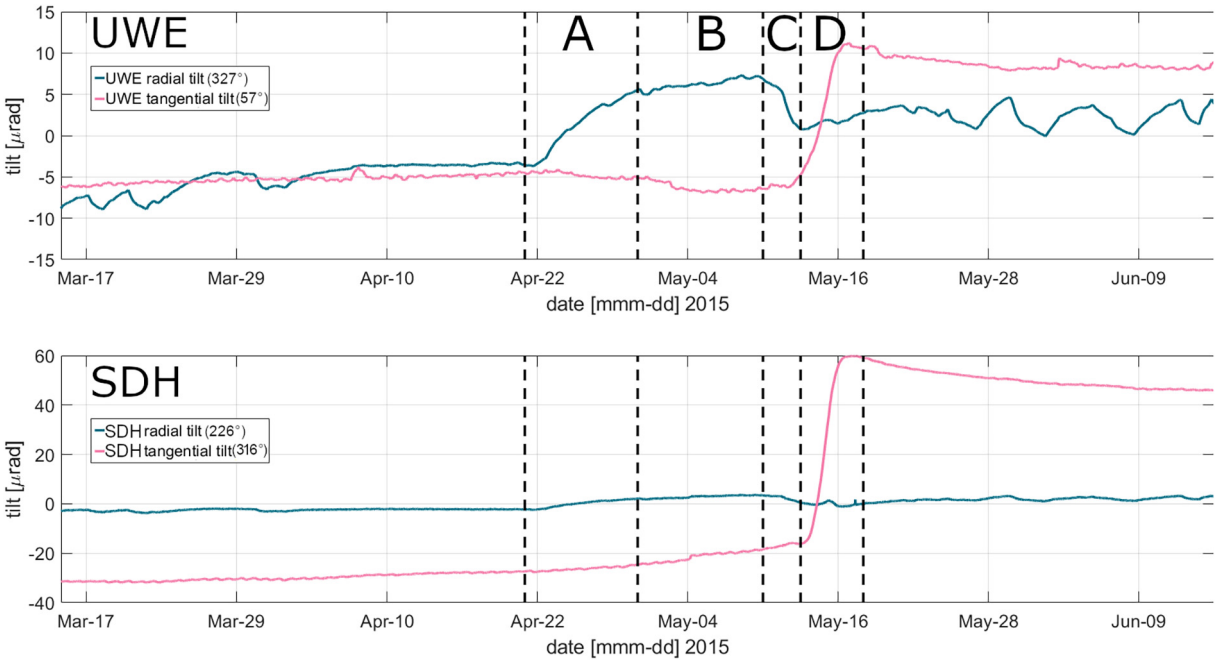

Fig. 5. Tilt time series from 2015 to 03-15 to 2015-06-15 from the UWE (top) and SDH (bottom) instruments. Orientation given in degrees clockwise from North. Dashed vertical lines separate the different stages of the May 2015 event.

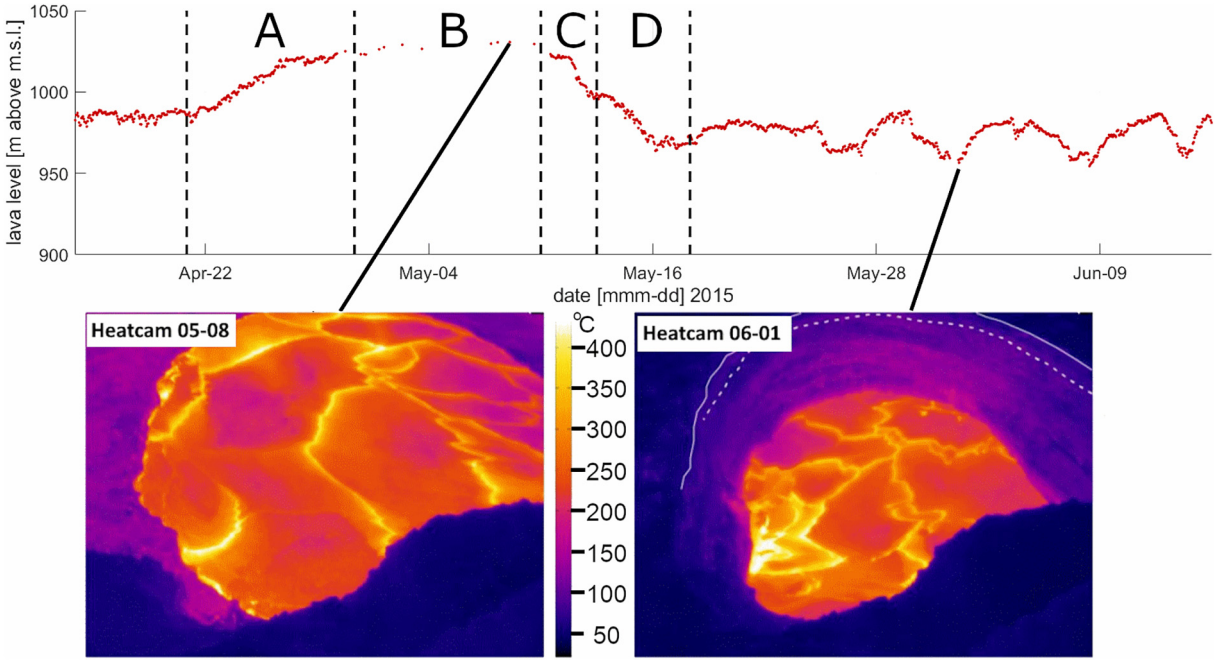

Fig. 6. Lava lake level variation from April 15 to June 15, 2015. Images from the infrared camera are shown with a line to the day of recording. The new and former edge of the summit eruptive vent are highlighted in the June 1 image by solid and dashed white lines, respectively.

displacements using weighted least squares resulting in the difference in LOS displacement between the stable periods:

$$\begin{bmatrix} \widehat{\varphi}_x^{zero} \\ \widehat{\varphi}_x^{offset} \end{bmatrix} = \left(A^T W A\right)^{-1} A^T W \widehat{\varphi}_x^{def}, \quad (1)$$

where $\widehat{\varphi}_x^{zero}$ is the near-zero mean LOS displacement of pixel x associated with the pre-event ("stable") period, and $\widehat{\varphi}_x^{offset}$ is the LOS displacement that occurred between the two stable periods – the "transition" period (e.g. April 9, 2015 - June 8, 2015 for descending track, and February 11, 2015 - June 11, 2015 for ascending track). Design matrix A is of the form (SP: Stable Period, TP: Transition Period):

$$A = \begin{bmatrix} \overbrace{1 \cdots 1}^{SP1} & \overbrace{0 \cdots 0}^{TP} & \overbrace{0 \cdots 1}^{SP2} \\ 0 \cdots 0 & 0 \cdots 0 & 1 \cdots 1 \end{bmatrix}^T, \quad (2)$$

Weight matrix W is a diagonal matrix filled with the reciprocal of the variance in the coherence of all PS pixels per interferogram. $\widehat{\varphi}_x^{def}$ is the

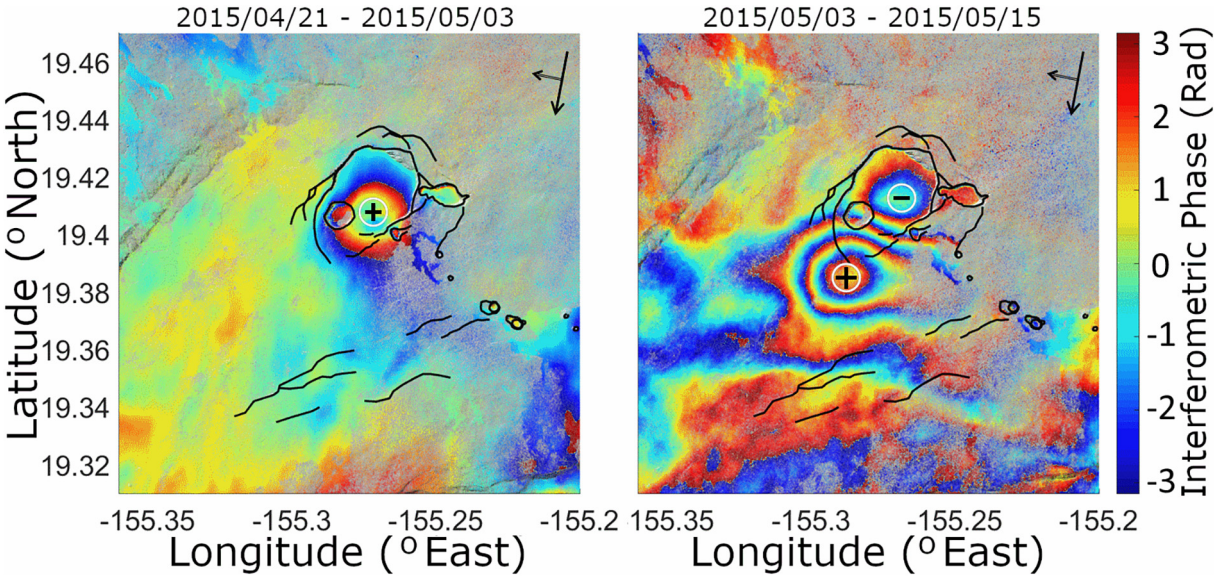

Fig. 7. Temporally consecutive Sentinel-1 interferograms showing deformation in Kīlauea's summit region before and during the May 2015 summit intrusion. Both interferograms are from the descending orbit. Left: Line-Of-Sight (LOS) displacement from April 21, 2015 to May 3, 2015. Right: LOS displacement from May 3, 2015 to May 15, 2015. The black arrows in the top right corner show the orbit path and look direction; 2π phase change equals 2.8 cm of LOS deformation. The white circles with'+' or'-' indicate movement toward and away from the satellite, respectively.

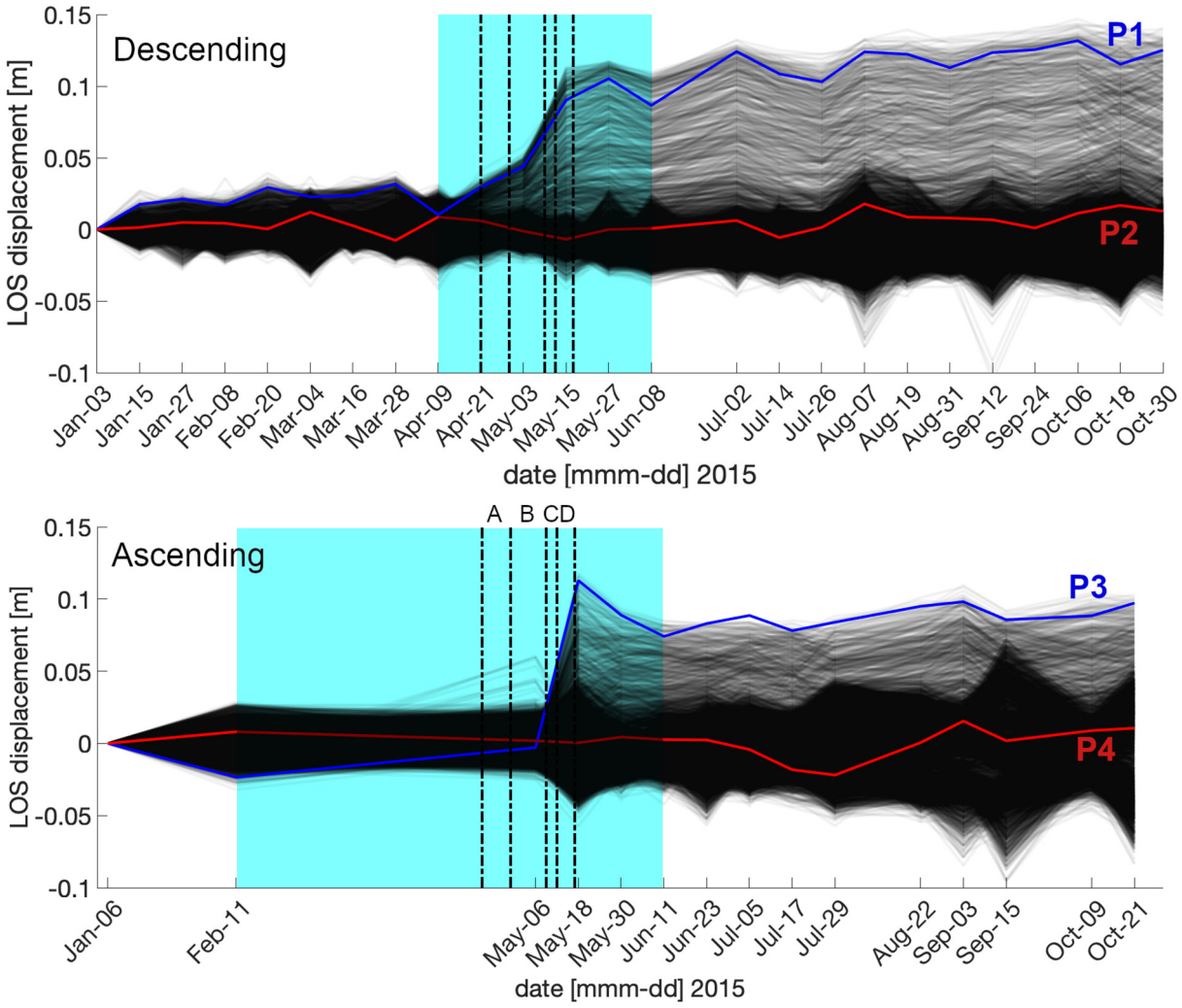

Fig. 8. Time series of LOS displacement of 5000 randomly selected PS pixels from the descending set (top) and ascending set (bottom). The red highlighted pixels are examples of PS pixels without significant deformation in the LOS of the satellite. The blue highlighted pixels are examples of significant LOS deformation. The locations of pixels P1–4, are shown in Fig. 9. The light blue area shows the period for each data set over which LOS deformation due to the April–May 2015 event was calculated (e.g. the "transition" period). The dates on the x-axis show the acquisition dates. The vertical dashed lines separate stages A-D.

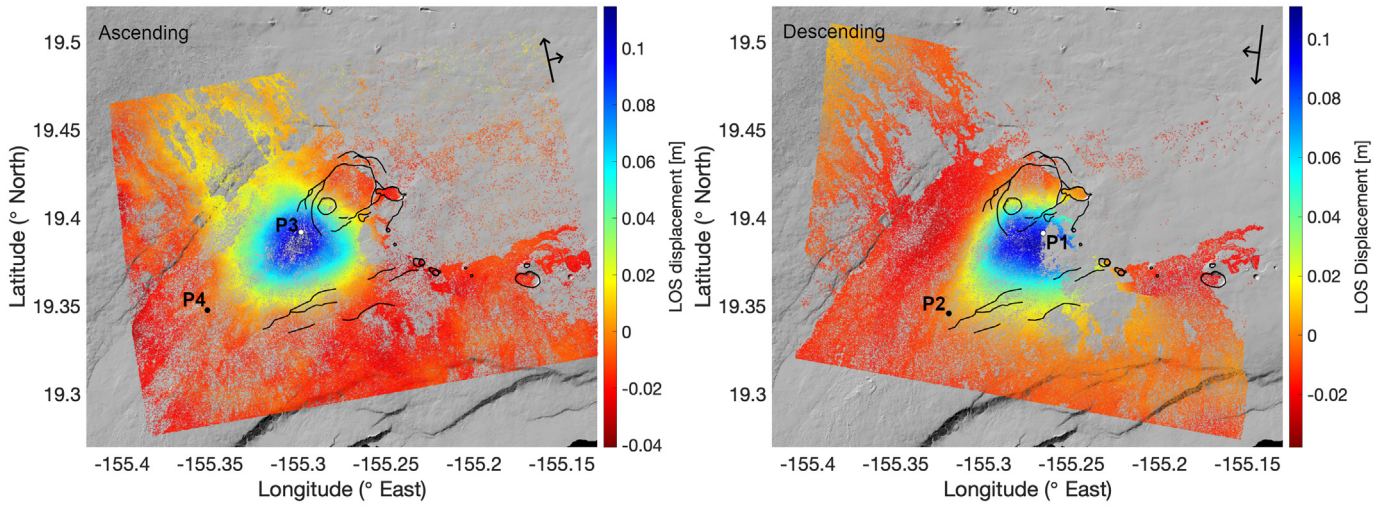

Fig. 9. LOS displacement of ascending (left) and descending (right) stacks over their respective transition periods (light blue areas in Fig. 8). Major craters and faults are indicated by black lines. The displacement time series for points P1–4 are highlighted in Fig. 8.

time series of LOS displacement estimated from StaMPS (See Fig. 8). This method estimates the total LOS displacement ($\hat{\varphi}_x^{offset}$) that occurred between the two stable periods. We call this the LOS displacement during the transition period. This improves the estimate of the total deformation during the short transition period compared to other commonly used methods, like: 1) deformation rate estimates, which, in this case, suffer from a lack of acquisitions during the period of deformation or 2) single interferograms, which could contain signals not associated with the April–May 2015 activity. The total LOS displacement accumulated during the transition period is displayed for both the ascending and descending data sets (Fig. 9).

Both ascending and descending displacement maps clearly show uplift of the south caldera (Fig. 9). The small-scale deformation inside the caldera visible in individual interferograms (Fig. 7) disappears in these deformation estimates. This indicates that the deformation centered on the HMMR was mostly transient and not permanent. The LOS displacement during the transition period, combined with GNSS displacements from April 21, 2015 to May 17, 2015, are used for the model inversion.

3. Deformation model inversion

We apply inverse models to estimate deformation source geometry, size, position and pressure/volume change using the GBIS software (Bagnardi and Hooper, 2018), with the surface deformation captured by GNSS (Fig. 4, bottom) and LOS deformation (Fig. 9) as inputs.

The boundary conditions are set taking into account the local geology and the previously proposed locations of the reservoirs (Poland et al., 2014; Jo et al., 2015; Baker and Amelung, 2012; Anderson et al., 2015). More detailed information on the modeling can be found in the supplementary information (Text S3, Table S3).

The main source of the observed deformation is located in the south caldera region, and so we start our modeling by assuming a deformation source located beneath that area. Previous deformation in this location has been modeled as 1) a point source (or Mogi model) (Mogi, 1958), 2) a planar opening (Okada, 1992), used at Kīlauea by (Baker and Amelung, 2012; Poland et al., 2014; Wauthier et al., 2016) and 3) an ellipsoidal source (Yang et al., 1988), used to model the 2015 deformation by Jo et al. (2015). We evaluate these model geometries (Figs. 10 and 11) and use the sum of squared residuals (SSR) (Table 1) to determine which model performs best.

The SSR values for the models are 39.15, 46.72, and 35.19 for the point source, sub-horizontal sill source and ellipsoidal source, respectively. The parameter values and 95% confidence intervals are given in Table 1. The ideal model solution has a volume change of $5.39 \cdot 10^6$ m^3, $5.98 \cdot 10^6$ m^3, and $7.80 \cdot 10^6$ m^3 for the point source, sill source, and ellipsoidal source, respectively, indicating the volume of the May 2015 intrusion into the SCR. In total, about $1.76 \cdot 10^6$ m^3 drained from the Halema'uma'u lava lake (see Section 2.4), which is less than 13 of the estimated intruded volume. The parameters describing the sill source displayed multi-modal behavior (see supplementary information GBIS_report_SILL.pdf), similar to those found by Jo et al., (2015). This, together with the higher SSR value, make the sill source an undesirable geometry for this event. Fig. 11 shows that the point source was the most inaccurate in replicating the observed GNSS displacements. Additionally, the geometry of the point source is inherently unnatural, being a non-physical source. Because of that, we also tested for a spherical source (McTigue, 1987). One of the parameters of the spherical source, the radius, consistently approaches the maximum boundary condition during inversion (see supplementary information GBIS report SPHEROID.pdf), indicating poor model convergence. The unnatural geometry of the point source and the poor model convergence of the spherical source make them poor candidates as source geometries for this event. We therefore favor the ellipsoidal model solution to describe the deformation centered on the SCR.

Jo et al. (2015) also used an ellipsoidal source to model the deformation in the south caldera region. Their optimal model solution closely resembles our optimal ellipsoidal source solution, and both are aligned with the strike of the SWRZ.

After model results for the main deformation signal (SCR source) are removed, visual inspection of the residual deformation (Fig. 10 C, E, G, J, L, N) suggests that another source, located within the summit caldera, was active during this time period.

The monitoring network, especially the tilt and lava level variations, show that pressure within the HMMR source fluctuated significantly during the April–May activity. The overall deformation is captured by the residuals shown in Fig. 10. To model the residual deformation, each of the optimal solutions (Table 1) was fixed, and a point source model, which is consistent with past models for the HMMR source (Anderson et al., 2015; Poland et al., 2014; Poland et al., 2009; Baker and Amelung, 2012), was added. Boundary conditions were chosen to approximate the bounds of the HMMR found previously (Baker and Amelung, 2012; Anderson et al., 2015; Poland et al., 2014). The optimal model solutions and 95% confidence intervals for each of the added point source models are shown in Table 2. The use of a two-source model reduces the SSR in all cases. The combination of a HMMR point

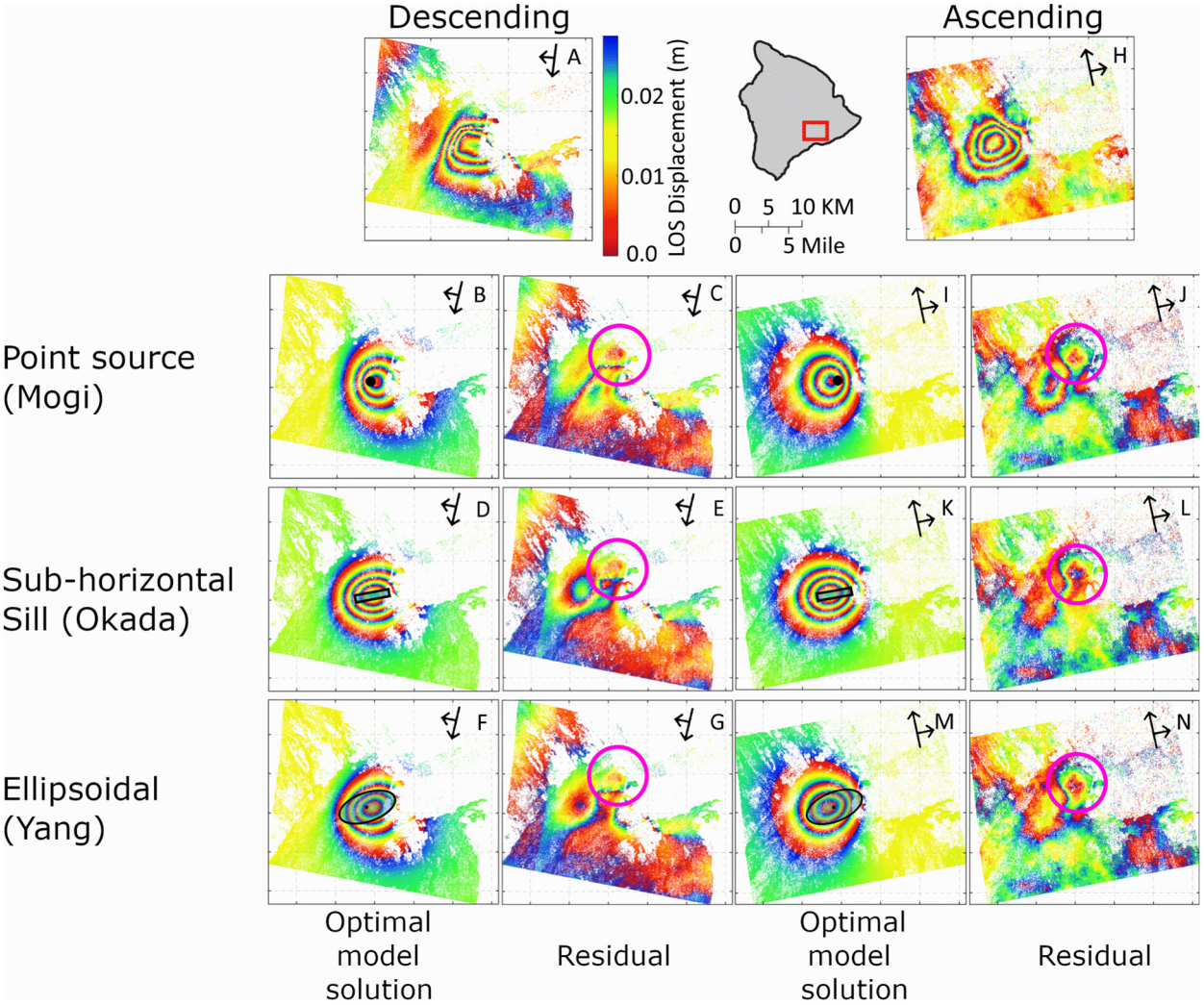

Fig. 10. Observed (A & H), modeled (B, D, F, I, K, M), and residual (C, E, G, J, L, N) wrapped LOS displacement spanning the May 2015 intrusion (defined by the blue shading in Fig. 8). A-G and H-M show the descending and ascending stacks, respectively. Images B, C, I, J refer to the point source model, for which the location is indicated by a black dot in B & I. Images D, E, K, L refer to the sill-like source, for which the outline is shown in D & K. Images F, G, M, N refer to the ellipsoidal source, for which the outline is shown in F & M. The colour bar and scale next to A are used for all figures. The magenta circles indicate a region of residual deformation inside the summit caldera.

source with the SCR point source, sub-horizontal sill source, and ellipsoidal source give SSRs of 38.94, 46.16, and 34.06, respectively. The greatest improvement in SSR is thus the combination of the ellipsoidal source for the SCR with a point source for the HMMR. The location, just east of Halema'uma'u crater, and depth, about 1.5 km, of the HMMR source is consistent with previous studies (e.g., Baker and Amelung, 2012; Poland et al., 2014, 2019; Anderson et al., 2015).

4. Discussion

In the following section we present a schematic representation of our interpretation for all available observations, which we use to explain the order of events that occurred at Kīlauea during April–May 2015. We then discuss the possible causes of this unusual activity and the consequences for our understanding of Kīlauea's magma plumbing system.

4.1. Explanation of events

Based on the variety of geodetic data and models, we developed a schematic interpretation (Fig. 12) depicting stages A-D of Kīlauea's April–May 2015 activity. During stage A, surface deformation observed by GNSS, tilt and InSAR indicates inflation centered around the eastern edge of Halema'uma'u crater (Figs. 4, 5, and 7). Increased earthquake activity, centered around this region at depths of 1–3 km (Fig. 3), and the rise in lava level are consistent with increased pressure within the HMMR, which is located approximately 1.5 km below the eastern edge of Halema'uma'u crater. Stage B is defined by only minor surface deformation centered about 1.5 km southeast of Halema'uma'u crater, near Keanakāko'i crater (Fig. 4). Increased seismic activity is observed in the upper ERZ and south caldera region (Fig. 3). Baker and Amelung (2012) point out that increased seismic activity in the upper ERZ can be associated with a magma storage area located southeast of the caldera at a depth of 3.4 km, referred to as the Keanakāko'i reservoir by Poland et al. (2014), although Wauthier et al. (2019) argue that upper ERZ seismicity may only reflect general summit pressurization, and not magma transport. Poland et al. (2014) proposed that inflation of the Keanakāko'i region represents temporary storage of magma at the interface between the summit and ERZ magmatic systems. The observed LOS displacement signal near Keanakāko'i crater in Fig. 7 might represent such temporary magma storage. The deformation is not present in the LOS displacements that span the entirety of the April–May 2015 activity (Fig. 9), confirming the transient nature of the deformation.

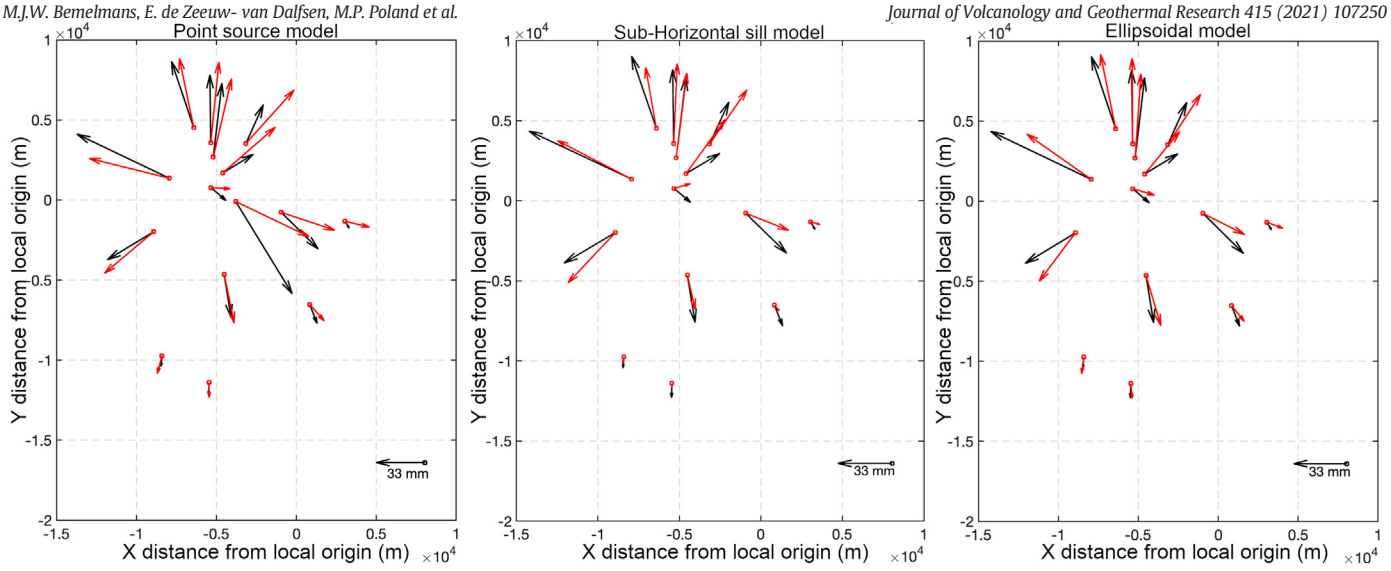

Fig. 11. Comparison of horizontal GNSS displacements (black: observations; red: model), spanning April 21, 2015 to May 17, 2015, for A) the point source model, B) the sill-like model, C) the ellipsoidal model. Output generated using the GBIS software. The outlined red squares are the summit GNSS stations shown in Fig. 1. Uncertainty ellipses are omitted for clarity and are shown in Fig. 4.

Stage C saw a lava level drop and surface deformation indicative of deflation of the HMMR (Figs. 4, 5, and 6) The earthquakes that occurred during this stage were mostly located in the south caldera region (Fig. 3), hinting at activity of the SCR. The drop in lava level, which acts as a proxy for pressure decrease of the HMMR (Patrick et al., 2015), and the increased seismic activity in the SCR could be explained by a hydraulic link between the HMMR and the SCR, as proposed by Poland et al. (2014) as part of the interconnected nature of Kīlauea's summit and rift zone magmatic systems. Stage D sees a further drop in lava level after a day of stability (see Fig. 6), and significant surface deformation is indicative of inflation of the SCR (Figs. 4, 5, and 7). The simultaneous drop in lava level and inflation of the SCR suggests that deflation of the HMMR continued from stage C to stage D as magma moved away from the HMMR into the SCR.

Table 1
Optimal model parameter results and 95% confidence intervals for the SCR. Depth is given in meters below mean elevation of the InSAR footprint in Fig. 9 (990.4 m above mean sea level).

Point source	value$^{[\text{confidence interval}]}$
Longitude (°)	$-155.284^{[-155.285,-155.283]}$
Latitude (°)	$19.386^{[19.385,19.387]}$
Depth (m)	$3370^{[3221,3548]}$
ΔV ($\cdot 10^6 m^3$)	$5.39^{[4.88,5.94]}$
SSR (m^2)	39.15
Sill source	**value$^{[\text{confidence interval}]}$**
Longitude (°)	$-155.263^{[-155.266,-155.260]}$
Latitude (°)	$19.390^{[19.386,19.392]}$
Depth (m)	$3993^{[3804,4283]}$
Length (m)	$675^{[250,1457]}$
Width (m)	$4870^{[4236,5399]}$
Dip (°)	$-2.0^{[-5.5,1.4]}$
Strike (°)	$-10.5^{[-17.3,-1.8]}$
Opening (m)	$1.8^{[0.7,4.9]}$
Optimal model ΔV ($\cdot 10^6 m^3$)	5.98
SSR (m^2)	46.72
Ellipsoidal source	**value$^{[\text{confidence interval}]}$**
Longitude (°)	$-155.287^{[-155.289,-155.285]}$
Latitude (°)	$19.3857^{[19.3844,19.3867]}$
Depth (m)	$2832^{[2646,3075]}$
Major axis (m)	$3687^{[3194,4289]}$
a/b (−)	$0.496^{[0.148,0.681]}$
Strike (°)	$249.7^{[241.0,258.2]}$
plunge (°)	$2.342^{[-3.314,8.091]}$
$\frac{\Delta P}{\mu}$ ($\cdot 10^{-4}$)	$1.15^{[0.411,14.6]}$
Optimal model ΔV ($\cdot 10^6 m^3$)	7.80
SSR (m^2)	35.19

4.2. Cause of changes in activity at Kīlauea

The deformation sequence observed during the May 2015 event started at the HMMR. The observed build up of pressure was due to an imbalance between magma influx and regular drainage to the ERZ eruptive vent, as postulated by Dzurisin and Poland (2018). The sudden onset of HMMR inflation suggests that something changed abruptly,

Table 2
Optimal model parameter results and 95% confidence intervals for the HMMR. Depth is given in meters below mean elevation of the InSAR footprint in Fig. 9 (990.4 m above mean sea level). Parameters for the corresponding SCR source model are shown in Table 1.

SCR = point source	value$^{[\text{confidence interval}]}$
Longitude (°)	$-155.281^{[-155.304,-155.278]}$
Latitude (°)	$19.413^{[19.410,19.428]}$
Depth (m)	$1559^{[1352,3874]}$
ΔV (m^3)	$-180{,}533^{[-896032,-113715]}$
SSR (m^2)	38.94
ΔSSR	0.21
SCR = sill source	**value$^{[\text{confidence interval}]}$**
Longitude (°)	$-155.271^{[-155.284,-155.262]}$
Latitude (°)	$19.407^{[19.404,19.421]}$
Depth (m)	$518^{[754,3271]}$
ΔV (m^3)	$-11{,}920^{[-249382,-11113]}$
SSR (m^2)	46.16
ΔSSR	0.56
SCR = ellipsoidal source	**value$^{[\text{confidence interval}]}$**
Longitude (°)	$-155.273^{[-155.280,-155.268]}$
Latitude (°)	$19.410^{[19.407,19.417]}$
Depth (m)	$1438^{[945,2623]}$
ΔV (m^3)	$-108{,}626^{[-289236,-37643]}$
SSR (m^2)	34.06
ΔSSR	1.13

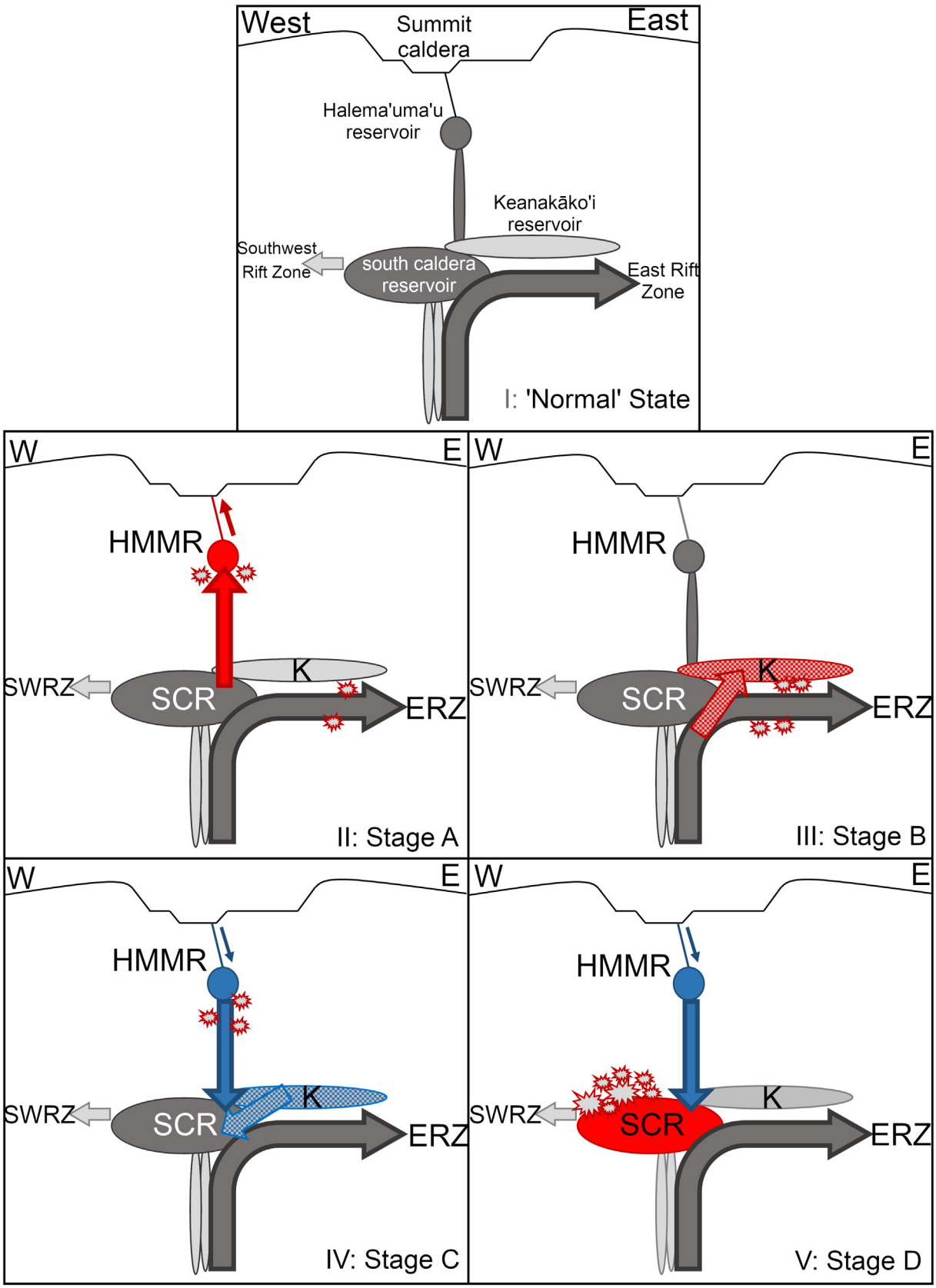
West
Summit caldera
East
Halema'uma'u reservoir
Keanakāko'i reservoir
Southwest Rift Zone
south caldera reservoir
East Rift Zone
I: 'Normal' State
W
E
HMMR
K
SWRZ
SCR
ERZ
II: Stage A
III: Stage B
IV: Stage C
V: Stage D

causing the build up of pressure. This imbalance could be caused by at least 4 mechanisms: 1) an increase in the magma supply rate, 2) lowered efficiency of the ERZ conduit, which is the primary drainage pathway for the summit plumbing system, 3) filling of void space near the HMMR and SCR to the extent that no more void space existed and magma was routed toward pressurizing the existing storage reservoirs, or 4) a combination of these processes.

Mechanism 1, an increase in the magma supply rate, was also observed between 2003 and 2007 (Baker and Amelung, 2012; Poland et al., 2014; Anderson and Poland, 2016) before subsequently dropping below 2003 levels between 2007 and 2012 (Poland et al., 2014; Anderson and Poland, 2016). Dzurisin and Poland (2018) hint at a possible increase between 2012 and 2015, bringing the magma supply rate back to pre-2003 levels by the end of that period. The short duration and sudden onset of the May 2015 event could be explained by a short-lived surge in magma supply on top of a gradual increase between 2012 and 2015.

Mechanism 2, a reduction in efficiency of the ERZ conduit, could be caused by stress perturbations in the upper ERZ (Chouet and Dawson, 2013) due to inflation/ deflation of the area or movement of the south flank. Sudden (partial) closure of the ERZ conduit or eruptive vent would also result in magma backing up toward the summit. This has been suggested for other summit inflation events (Orr et al., 2015). However, no change in the ERZ eruption rate was found in correspondence to the April–May 2015 summit activity (Patrick et al., 2019); therefore, mechanism 2 is not a likely cause of the May 2015 intrusion.

Mechanism 3, filling of void space in the summit region, could have caused the observed deformation. If the magma supply rate remained constant and was split between filling void space and feeding the ERZ eruption, then when the available void space ran out, this part of the magma supply would contribute to a pressure increase at the summit. Relative microgravity surveys could have helped to shed light on the sub-surface mass and density changes which occurred during the May 2015 event. This has proven effective at Kīlauea in the past (Johnson et al., 2010; Bagnardi et al., 2014; Poland et al., 2019), with several authors suggesting filling or draining of void space to explain mass addition or subtraction in the subsurface without accompanying surface deformation. The closest microgravity surveys encompassing the May 2015 event were conducted in Oct/Nov 2012 and Sept 2015. Analysis of these data did not yield usable results (see supplemental information Text S4 and Fig. S4). This is mainly because microgravity change observed between these two surveys includes not only changes induced by the May 2015 event, but also those from the preceding 2.5 years. This stresses the importance of regular microgravity surveys in the area. Regardless, the rapid nature of the inflation onset in April 2015 argues against the gradual filling of void space, although it is a mechanism we cannot definitively discount.

Finally the May 2015 event could have been caused by a combination of these three mechanisms. The lower magma supply rate during 2010–2012 coincides with constriction of the ERZ conduit (Patrick et al., 2019). It is possible that during this period the ERZ conduit was narrowed, decreasing its maximum flow capacity. In April 2015, a steady increase in magma supply, which might have started in 2012, could have reached this maximum flow capacity, causing any additional magma supply to fill summit reservoirs. Alternatively, an increased magma supply between 2012 and 2015 could have slowly filled all available void space in the summit region. When this space was no longer available, the summit began to inflate. This pressure increase was eventually alleviated by an intrusion that expanded the SCR.

The evidence presented in Dzurisin and Poland (2018) suggests an increased magma supply rate; however, without an estimate of short-term magma supply rate or the filling rate of void space, the ultimate mechanism for the imbalance between supply rate and eruption rate during April–May 2015 remains speculative.

5. Conclusions

Data from GNSS, tilt, lava lake level, seismicity and InSAR allow us to distinguish four distinct stages of deformation associated with Kīlauea's May 2015 summit intrusion. These stages are linked to the imbalance in magma supply and discharge rate to/from the shallow plumbing system of Kīlauea Volcano. The May 2015 event started with pressurization and inflation of the HMMR, probably caused by an increase in magma supply rate to the shallow plumbing system. Possibly this process was aided by the ultimate filling of void space in the subsurface and/or reduced efficiency of the ERZ conduit after a period of lower magma supply from 2010 to 2012. The ultimate outcome of this imbalance was a magmatic intrusion into the SCR following a period of shallow summit inflation centered on the HMMR.

The analysis of ground and space geodetic data relating to the May 2015 event resulted in a significantly improved understanding of the evolution of the volcanic activity and the resulting deformation, which has been linked to the activity of two or possibly three interconnected magma reservoirs in the shallow pluming system of Kīlauea Volcano. The processes that were ultimately responsible for the imbalance in magma supply and withdrawal, however, remain speculative. More frequent microgravity campaign surveys would help to understand and quantify these processes and address this question.

Declaration of Competing Interest

All authors declare that they have no competing interest.

Acknowledgments

We are grateful to the Mathematical Geodesy and Positioning department at Delft University of Technology led by Prof. Dr. Ir. Ramon Hanssen for their support and for the use of their computing facilities. Staff at the Royal Netherlands Meteorological Institute also provided insightful comments during the research process for which we are grateful. The GNSS data are archived at UNAVCO (https://www.unavco.org/), Sentinel-1 data are available from the ESA SCIHUB. Seismic data are archived at IRIS (https://www.iris.edu/hq/), and earthquake locations are at National Earthquake Information Centre (NEIC). The tilt and gravimetry data were provided by the Hawaiian Volcano observatory. Ownership of these data belongs with them. We use StaMPS (Hooper et al., 2007) and GBIS (Bagnardi and Hooper, 2018) for SAR data processing

Fig. 12. Schematic of the behavior of Kīlauea during the different stages of the May 2015 event. The cross sections run from west to east and show surface features of Kīlauea volcano (before the major 2018 collapse) along with a simplified representation of the proposed plumbing system of the volcano (Baker and Amelung, 2012; Poland et al., 2014). Red colors indicate pressurization/inflation, blue colors indicate depressurization/deflation, and dark grey indicates areas filled with magma but not actively pressurizing or depressurizing. I) The general state of the plumbing system, with the magma supplied from below mostly going into the ERZ without significant deformation in the summit region. The transport of magma to the ERZ did not noticeably change during the May 2015 event (Patrick et al., 2019). Because of that, the dark-grey arrow is present in all following panels. The path to the 2008–2018 summit lava lake is also shown in dark-grey to represent the presence of magma when no significant variation in lava lake level was observed. II) Activity during stage A, with pressurization of the HMMR. III) Stage B, with possible temporary storage of magma in the Keanakāko'i reservoir (shaded half red). IV) Stage C, draining of the HMMR and possibly the Keanakāko'i reservoir (shaded half blue), with magma moving into the SCR. V) Stage D, Inflation of the SCR, with continued draining from the HMMR. The schematic location of seismic activity is shown with jagged polygons, whereby the number of polygons indicates the level of activity. Note that their position with respect to the plumbing system is not reflecting any interpretation from the data. Schematic is not to scale.

and modeling. We are grateful to the staff of the Hawaiian Volcano Observatory for their support of geophysical measurements at Kīlauea, and for the collaboration and support of Hawai'i Volcanoes National Park, within which all data were collected. TerraSAR-X and COSMO-SkyMed SAR data were used to form interferograms for determining free-air corrections on gravity measurements. The SAR data were provided by the Deutsches Zentrum für Luft- und Raumfahrt (German Aerospace Center) and Agenzia Spaziale Italiana (Italian Space Agency) via the Hawaii Supersite.

Appendix A. Supplementary data

Supplementary data to this article can be found online at https://doi.org/10.1016/j.jvolgeores.2021.107250.

References

Anderson, K.R., Poland, M.P., 2016. Bayesian estimation of magma supply, storage, and eruption rates using a multiphysical volcano model: Kīlauea Volcano, 2000–2012. Earth Planet. Sci. Lett. 447, 161–171.

Anderson, K.R., Poland, M.P., Johnson, J.H., Miklius, A., 2015. Episodic Deflation–Inflation Events at Kīlauea Volcano and Implications for the Shallow Magma System. chapter 11. American Geophysical Union (AGU), pp. 229–250.

Bagnardi, M., Hooper, A., 2018. Inversion of surface deformation data for rapid estimates of source parameters and uncertainties: a bayesian approach. Geochem. Geophys. Geosyst. 19 (7), 2194–2211.

Bagnardi, M., Poland, M.P., Carbone, D., Baker, S., Battaglia, M., Amelung, F., 2014. Gravity changes and deformation at Klauea Volcano, Hawaii, associated with summit eruptive activity, 2009–2012. J. Geophys. Res. Solid Earth 119 (9), 7288–7305.

Baker, S., Amelung, F., 2012. Top-down inflation and deflation at the summit of Kīlauea Volcano, Hawai'i observed with InSAR. J. Geophys. Res. Solid Earth 117 (B12).

Carbone, D., Poland, M.P., Patrick, M.R., Orr, T.R., 2013. Continuous gravity measurements reveal a low-density lava lake at Kīlauea Volcano, Hawai'i. Earth Planet. Sci. Lett. 376, 178–185.

Cervelli, P.F., Miklius, A., 2003. The shallow magmatic system of Kīlauea Volcano. US Geol. Surv. Prof. Pap. 1676, 149–163.

Chouet, B., Dawson, P., 2013. Very long period conduit oscillations induced by rockfalls at Kīlauea Volcano, Hawaii. J. Geophys. Res. Solid Earth 118 (10), 5352–5371.

Dzurisin, D., Poland, M.P., 2018. Magma supply to Klauea Volcano, Hawai'i, from inception to now: Historical perspective, current state of knowledge, and future challenges. Field Volcanol. 538, 275.

Farr, T.G., Rosen, P.A., Caro, E., Crippen, R., Duren, R., Hensley, S., Kobrick, M., Paller, M., Rodriguez, E., Roth, L., Seal, D., Shaffer, S., Shimada, J., Umland, J., Werner, M., Oskin, M., Burbank, D., Alsdorf, D., 2007. The shuttle radar topography mission. Rev. Geophys. 45 (2).

Fiske, R.S., Kinoshita, W.T., 1969. Inflation of Kilauea volcano prior to its 1967-1968 eruption. Science 165 (3891), 341–349.

Hooper, A., Zebker, H., Segall, P., Kampes, B., 2004. A new method for measuring deformation on volcanoes and other natural terrains using InSAR persistent scatterers. Geophys. Res. Lett. 31 (23).

Hooper, A., Segall, P., Zebker, H., 2007. Persistent scatterer interferometric synthetic aperture radar for crustal deformation analysis, with application to VolcÃ¡n Alcedo, GalÃ¡pagos. J. Geophys. Res. Solid Earth 112 (B7).

Jo, M.-J., Jung, H.-S., Won, J.-S., 2015. Detecting the source location of recent summit inflation via three-dimensional InSAR observation of Kīlauea volcano. Remote Sens. 7 (11), 14386–14402.

Johnson, D.J., Eggers, A.A., Bagnardi, M., Battaglia, M., Poland, M.P., Miklius, A., 2010. Shallow magma accumulation at Kīlauea Volcano, Hawai'i, revealed by microgravity surveys. Geology 38 (12), 1139–1142.

Klein, F.W., Koyanagi, R.Y., Nakata, J.S., Tanigawa, W.R., 1987. The seismicity of Kīlauea's magma system. US Geol. Surv. Prof. Pap. 1350 (2), 1019–1185.

McTigue, D., 1987. Elastic stress and deformation near a finite spherical magma body: resolution of the point source paradox. J. Geophys. Res. Solid Earth 92 (B12), 12931–12940.

Mogi, K., 1958. Relations between the eruptions of various volcanoes and the deformations of the ground surfaces around them. Earthq. Res. Inst. 36, 99–134.

Neal, C.A., Brantley, S.R., Antolik, L., Babb, J.L., Burgess, M., Calles, K., Cappos, M., Chang, J.C., Conway, S., Desmither, L., Dotray, P., Elias, T., Fukunaga, P., Fuke, S., Johanson, I.A., Kamibayashi, K., Kauahikaua, J., Lee, R.L., Pekalib, S., Miklius, A., Million, W., Moniz, C.J., Nadeau, P.A., Okubo, P., Parcheta, C., Patrick, M.R., Shiro, B., Swanson, D.A., Tollett, W., Trusdell, F., Younger, E.F., Zoeller, M.H., Montgomery-Brown, E.K., Anderson, K.R., Poland, M.P., Ball, J.L., Bard, J., Coombs, M., Dietterich, H.R., Kern, C., Thelen, W.A., Cervelli, P.F., Orr, T., Houghton, B.F., Gansecki, C., Hazlett, R., Lundgren, P., Diefenbach, A.K., Lerner, A.H., Waite, G., Kelly, P., Clor, L., Werner, C., Mulliken, K., Fisher, G., Damby, D., 2019. The 2018 rift eruption and summit collapse of Kīlauea Volcano. Science 363 (6425), 367–374.

Okada, Y., 1992. Internal deformation due to shear and tensile faults in a half-space. Bull. Seismol. Soc. Am. 82 (2), 1018–1040.

Orr, T.R., Poland, M.P., Patrick, M.R., Thelen, W.A., Sutton, A.J., Elias, T., Thornber, C.R., Parcheta, C., Wooten, K.M., 2015. Kīlauea's 5–9 March 2011 Kamoamoa Fissure Eruption and Its Relation to 30+ Years of Activity From Pu 'u 'Ō 'ō. chapter 18. American Geophysical Union (AGU), pp. 393–420.

Patrick, M.R., Anderson, K.R., Poland, M.P., Orr, T.R., Swanson, D.A., 2015. Lava lake level as a gauge of magma reservoir pressure and eruptive hazard. Geology 43 (9), 831–834.

Patrick, M., Orr, T., Anderson, K., Swanson, D., 2019. Eruptions in sync: improved constraints on Kīlauea Volcano's hydraulic connection. Earth Planet. Sci. Lett. 507, 50–61.

Poland, M.P., Sutton, A.J., Gerlach, T.M., 2009. Magma degassing triggered by static decompression at Kīlauea Volcano, Hawai'i. Geophys. Res. Lett. 36 (16).

Poland, M.P., Takahashi, T.J., Landowski, C.M., 2014. Characteristics of Hawaiian Volcanoes. Government Printing Office.

Poland, M.P., de Zeeuw-van Dalfsen, E., Bagnardi, M., Johanson, I.A., 2019. Post-Collapse Gravity increase at the Summit of Kīlauea Volcano, Hawai'i. Geophys. Res. Lett. 46 (24), 14430–14439.

Swanson, D.A., Houghton, B.F., Poland, M., Garcia, M., Camp, V., Grunder, A., 2018. Products, processes, and implications of Keanakāko 'i volcanism, Klauea Volcano, Hawai'i. Field Volcanology: A Tribute to the Distinguished Career of Don Swanson: Geological Society of America Special Paper. 538, pp. 159–190.

Traversa, P., Grasso, J.-R., 2010. How is Volcano Seismicity different from Tectonic Seismicity? Bull. Seismol. Soc. Am. 100 (4), 1755–1769.

Wauthier, C., Roman, D.C., Poland, M.P., 2016. Joint analysis of geodetic and earthquake fault-plane solution data to constrain magmatic sources: a case study from Kīlauea Volcano. Earth Planet. Sci. Lett. 455, 38–48.

Wauthier, C., Roman, D.C., Poland, M.P., 2019. Modulation of seismic activity in Kīlauea's upper East Rift Zone (Hawai 'i) by summit pressurization. Geology. 47 (9), 820–824.

Yang, X.-M., Davis, P.M., Dieterich, J.H., 1988. Deformation from inflation of a dipping finite prolate spheroid in an elastic half-space as a model for volcanic stressing. J. Geophys. Res. Solid Earth 93 (B5), 4249–4257.